■ **Supramolecular Polymers** | *Very Important Paper* |

Mechanistic Insights into Statistical Co-Assembly of Metal Complexes

Joao Paulo Coelho, Jonas Matern, Rodrigo Q. Albuquerque, and Gustavo Fernández*[a]

Abstract: Statistical copolymerization plays a key role in many biological and technological processes; however, mechanistic understanding of the formation of analogous supramolecular counterparts remains limited. Herein, we report detailed insights into the supramolecular co-assembly of two π-conjugated Pd^{II} and Pt^{II} complexes, which in isolation self-assemble into flexible fibers and nanodisks, respectively. An efficient single-step co-assembly into only one type of nanostructure (fibers or nanodisks) takes place if any of the components is in excess. In contrast, equimolar mixtures lead to Pd^{II}-rich fiber-like co-assemblies by a statistical co-nucleation event along with a residual amount of self-sorted nanodisks in a stepwise manner.

Statistical or random copolymerization plays a key role in multiple biological processes[1] and is a commonly used strategy to enhance the physical properties of technological materials in general.[2] In such polymers, the monomer residues are distributed within uneven sequences along the (covalent) molecular chain.[3] A similar approach based on the noncovalent association of different molecular entities has been already successfully employed in the development of novel supramolecular materials. For example, the groups of Meijer and Palmans,[4a–c] Yam,[4d] and Sugiyasu and Takeuchi,[4e] the latter making use of the seeded-growth approach,[5] have exploited this strategy to tune the stability, composition, and functionality of multicomponent self-assembled nanostructures. These systems often result in segregated molecular domains or blocks along the supramolecular chain where unlike monomer units show little interaction. On the other hand, statistical supramolecular co-polymers offer a complementary approach for building up nanostructures with novel, emergent physicochemical properties arising from a continuous and integrative multimolecular system. In a recent example, Palmans, Meijer, and co-workers relied on the effects of steric hindrance and side-chain incompatibility to efficiently create random supramolecular copolymers using ca. 10% of the bulky co-monomer.[6] Herein, we in-troduce a straightforward strategy to control the outcome of statistical co-assembly processes at any ratio by merely changing the nature of the metal ion while keeping an identical molecular design of the monomer units.

The systems investigated in this work are two hydrophobic OPE-based[7] dichloro(bis)pyridyl Pd^{II} and Pt^{II} complexes (compounds **1** and **2** in Scheme 1, see the Supporting Information for synthetic details), which have been reported by our group to self-assemble independently into supramolecular polymers in methylcyclohexane (MCH).[8] Their distinct molecular packing ((pseudo)parallel for Pd^{II} versus slipped stacks for Pt^{II}), particularly driven by the metal fragment, motivated us to investigate the feasibility of their supramolecular co-assembly. Such analysis proved difficult in MCH due to the rather low and close values of elongation temperatures (T_e) for **1** and **2** (281 vs. 290 K, respectively; Figure S1, Supporting Information). We thus selected a linear alkane solvent (decane), which, apart from enhancing the aggregation propensity of the systems,[9] enables a further differentiation between the T_e values. In contrast to MCH, this solvent induces a comparable pseudo-parallel arrangement for both target complexes **1** and **2** (vide infra).

Variable temperature (VT)-UV/Vis absorption spectroscopy in decane at 52 μM provided first insights into the self-assembly behavior of **1** and **2** in isolation (Figure 1). These results coincide with those previously observed for both independent complexes in MCH upon cooling: a bathochromic shift from 349 to 372 nm for **1**, and from 357 to 380 nm (with a shoulder at 397 nm) for **2** (Figures 1a and b, respectively). While both complexes are molecularly dissolved at 363 K, the spectral changes at 273 K can be assigned to the formation of self-assembled structures. By analogy with the behavior in MCH, the plot of fraction of aggregated species (α_{agg}) versus temperature, estimated by monitoring the spectral changes at 400 nm, revealed nonsigmoidal, sharp transitions (Figure 1 c).[10] Thermodynamic analysis of these curves using the cooperative equilibrium model[11] shed T_e values of 315 K for **1** and 298 K for **2**, respectively (for a detailed overview of the thermodynamic parameters, see Table S1, Supporting Information).

Interestingly, morphological analysis of the aggregates formed by **1** and **2** in decane, visualized by AFM on a silicon wafer, revealed marked differences between both complexes. While long twisted fibers with heights of 2.5±1 nm and several microns in length were observed for **1** (Figure 2a), discoidal structures (nanodisks) of unimolecular height (4±2 nm) and average diameter of 30±15 nm were obtained for **2** (Figure 2c). These discrete particle sizes for **2** are in good accordance with dynamic light scattering (DLS) measurements (Fig-

[a] Dr. J. P. Coelho, J. Matern, Dr. R. Q. Albuquerque, Prof. Dr. G. Fernández
Organisch-Chemisches Institut, Westfälische Wilhelms-Universität
Münster, Corrensstrasse 40, 48149 Münster (Germany)
E-mail: fernandg@uni-muenster.de
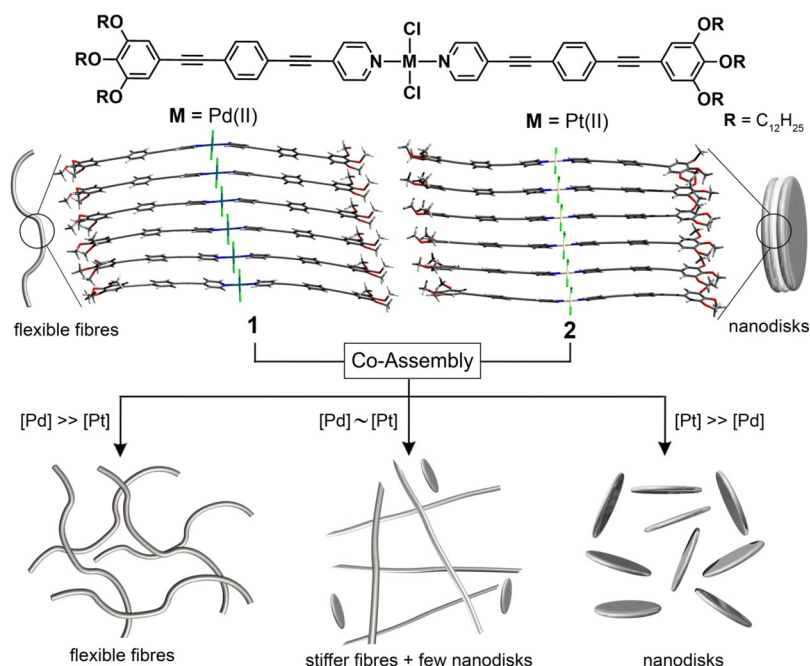
Scheme 1. Molecular structures of **1** and **2** and schematic representation of their self- and co-assembly processes at different ratios in decane. The hexameric stacks of **1** and **2** have been optimized using the dispersion-corrected PM6 method.
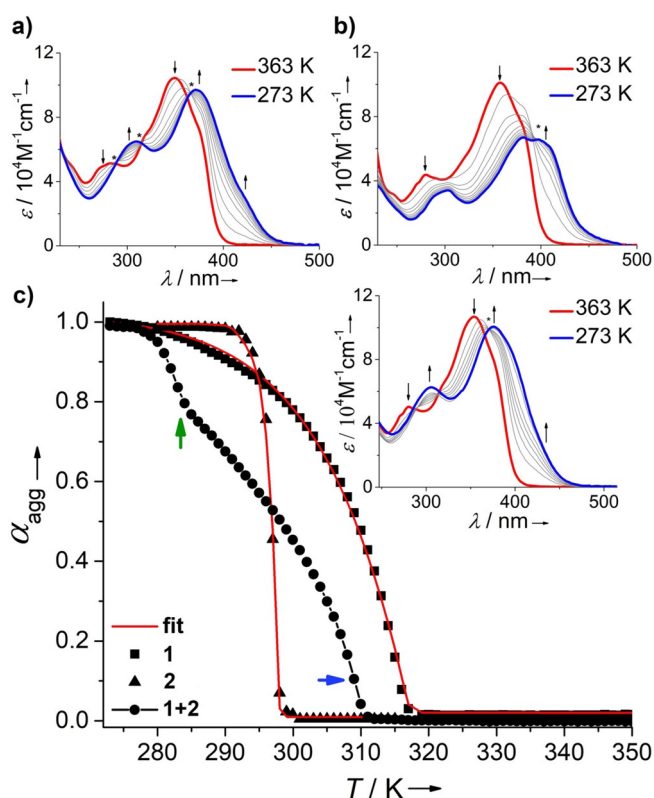
Figure 1. VT-UV/Vis spectra of **1** (a) and **2** (b) recorded from 363 to 273 K (1 K min^{-1}) at 52 μM in decane. c) Plots of α_{agg} versus T ($\lambda = 400$ nm) for **1** (■) **2** (▲) and an equimolar mixture of **1**+**2** (●) (the blue and green arrows indicate the T_e for the mixture of **1**+**2** and the temperature at which the second process begins, respectively). Inset: VT-UV/Vis spectra of the 1:1 mixture of **1**+**2** from 363 to 273 K in decane at 52 μM. Black arrows indicate spectral changes upon cooling and asterisks denote isosbestic points.

ure 2d). Particularly, the minor dependency of the values of the hydrodynamic radii (R_H) on the measuring angle suggests the lack of anisotropic nanostructures.[12] The marked difference in terms of aggregate morphology between **2** in MCH (fibers)[8b] and decane (disks) might be related to the poor solvation of monomeric units of **2** by decane molecules, leading to a sudden polymerization process in a very narrow temperature range upon cooling. This is evident from the sharp transition observed in the plot of α_{agg} versus T, in which full conversion from monomer to aggregates occurs within only 10 K. On the other hand, the considerably larger and strongly angle-dependent R_H values for **1** support the formation of long 1D fibers (Figure 2b).

VT-^{1}H NMR measurements (520 μM, [D$_{22}$]decane) for both complexes were performed to monitor the changes at the molecular level upon aggregation. Simultaneously, VT-UV/Vis cooling curves were also recorded at this higher concentration to allow a reliable comparison between both techniques. VT-^{1}H NMR upon cooling show a marked broadening and shielding of the aromatic resonances for both complexes in isolation, which is indicative of aggregation. At temperatures slightly higher than the T_e (ca. 338 K extracted from the VT-UV/Vis cooling curve) down to 303 K, the proton signals of the aromatic rings H$_{a–c}$ shift upfield, suggesting the involvement of these rings in aromatic interactions (Figure S2, Supporting Information). These shifts are much less marked for the outer protons (H$_d$), most likely indicating a rotational offset of the molecules in the stack caused by the steric demand of the alkoxy chains. Below 308 K, the severe broadening and disappearance of the signals is in agreement with an extended aggregation into fiber-like assemblies.[13] On the other hand, the spectra recorded under the same conditions for **2** (Figure S3, Supporting In-
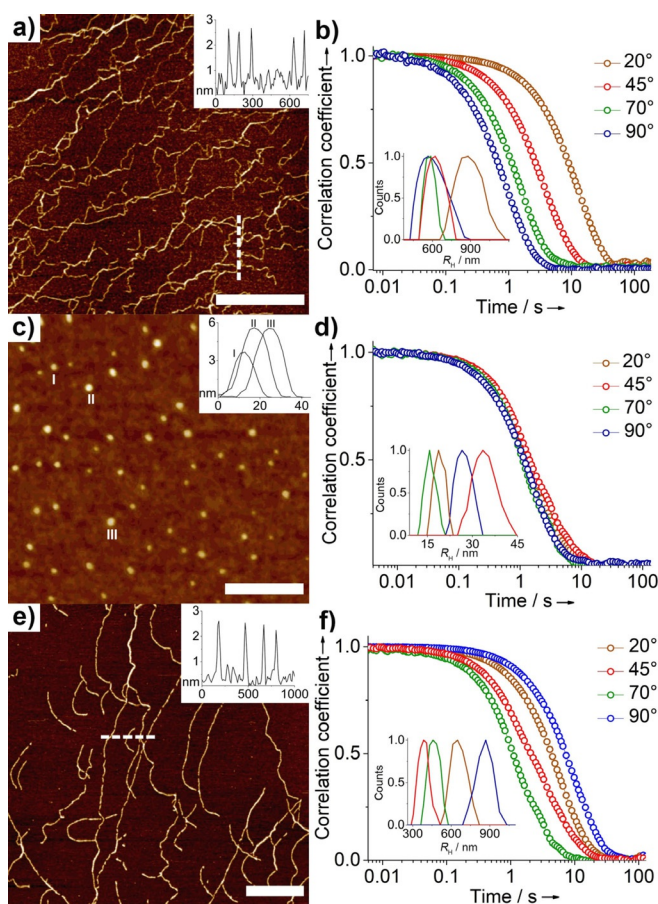
Figure 2. Height AFM images of **1** (a), **2** (c) and **1**+**2** (e) prepared by spin coating onto silicon wafer (scale bar = 1 μm). Cross-section analyses correspond to the white dashed lines. Normalized size distribution obtained from the autocorrelation functions of **1** (b), **2** (d), and **1**+**2** (f) at different angles. Samples **1** and **2** were prepared at 273 K, whereas **1**+**2** were prepared at 290 K.

formation) show a more pronounced shielding of the protons H_{a-c} compared to **1**, implying stronger π-stacking interactions. Interestingly, these signals shield and broaden at temperatures considerably higher than the T_e (ca. 308 K), which may be related to a pre-nucleation event into disordered short oligomers prior to the subsequent elongation.[14]

Based on the overall results, we propose a molecular packing for stacks of **1** and **2** (Scheme 1) using the dispersion-corrected PM6 method,[15a] which has been recently used to describe similar supramolecular assemblies.[15b] The stacking model of **1** displays a slightly slipped arrangement ($\theta = 17°$) with a weak rotational offset (Scheme 1 and Figure S4, Supporting Information), which is in line with the formation of twisted fibers as well as with previous UV/Vis and NMR spectroscopic studies. This effect can be related to the steric bulkiness of the chlorine ligands, which precludes an ideal parallel arrangement ($d_{Pd\cdots Pd} \approx 3.9$ Å) and enables short intermolecular contacts with the metal centers of adjacent molecules ($d_{Pd\cdots Cl} \approx 2.6$ Å). The calculations performed for **2** show a comparable (pseudo)parallel packing ($d_{Pt\cdots Cl} \approx 3.1$, $d_{Pt\cdots Pt} \approx 3.8$ Å); however, with a negligible rotational offset (Figure S5, Supporting Infor-

mation), which might explain the formation of discoidal nano-structures.

After analysis of the supramolecular polymerization of **1** and **2**, we next assessed the efficiency of their co-assembly under thermodynamic control by VT-UV/Vis and emission studies. Initially, an equimolar mixture of **1** and **2** at 52 μm in decane was heated to a molecularly dissolved state (363 K) and cooled down to 273 K by using a 1 K min⁻¹ rate to monitor the co-assembly process. Upon cooling, a bathochromic shift of the absorption maximum from 353 to 378 nm occurs (inset of Figure 1 c). Simultaneously, the shoulder at 280 nm shifts to approximately 305 nm. VT-photoluminescence studies using identical conditions show a more significant enhancement of the emission for the **1**+**2** mixture compared to the individual components (Figure S6, Supporting Information). These findings can be explained by the restricted molecular rotation of the OPE fragments induced by their planarization upon aggregation,[16] which appears to be stronger in the co-assembly. Interestingly, the cooling curve (plot of α_{agg} vs. T) extracted from VT-UV/Vis studies at a wavelength of 400 nm discloses two different regimes: the first transition occurs at a temperature of 308 K (marked with a blue arrow in Figure 1 c), followed by a second process at ca. 285 K (marked with a green arrow in Figure 1 c). Notably, the T_e associated with the first step is 7 K lower than that of the Pd^{II} complex in isolation (313 K), indicating that the presence of free Pt^{II} monomers delays the nucleation step of the Pd^{II} complex **1**. This behavior is characteristic of a co-nucleation event between both molecules[4a] that proceeds in a statistical manner. In the following elongation process between 308 and 285 K, the spectroscopic features of the mixture **1**+**2** are reminiscent of those of pure **1** (Figure S7a–e, Supporting Information). This is indicative of a social self-sorting dictated by **1** rather than a narcissistic aggregation of **1** and **2**. AFM imaging shows that only fibers and no discoidal structures (as those observed for **1** in isolation) are formed at 290 K (Figure 2e–f), which further supports the co-assembly of **1** and **2** during this first process.

Interestingly, a second regime is noticeable at temperatures between 285 and 273 K (marked with a green arrow in Figure 1 c). Most likely, at this lower temperature, a remaining amount of Pt^{II} monomers in solution has a higher propensity to self-recognize rather than to co-assemble with **1**, leading to a residual narcissistic self-polymerization of **2**. This is supported by the appearance of a shoulder at 397 nm, which is a characteristic feature of the self-aggregation of Pt^{II} moieties (Figure S7f–h, Supporting Information).[8b] In addition, the observation of a mixture of fibers and nanodisks at lower temperatures by AFM/TEM and the appearance of two distinct peaks corresponding to small and larger particle sizes in DLS validates this hypothesis (Figures S8 and S9, Supporting Information).

Additional evidence supporting the co-assembly was provided by the VT-¹H NMR measurements (Figure S10, Supporting Information). Apart from the expected behavior (broadening and shielding of the resonances of both **1** and **2** upon cooling), the spectra at low temperatures (below 303 K) shows a complete disappearance of the H_a protons of **1** only, but not of those from **2** (Figure S10, Supporting Information) even at

the lowest temperatures. These findings are in agreement with the proposed hypothesis that the initial co-assembled fibers are rich in Pd(II) monomers. At lower temperatures, however, the Pd(II) monomers are no longer available (they have been consumed to form the Pd-rich fibers) whereas the residual Pt(II) monomers have the only option to self-organize into the observed nanodisks.

Considering that the co-assembly process yields Pd-rich fibers, heteromeric stacks using a slight excess of Pd(II) monomers (four Pd(II) vs. two Pt(II) units) were optimized by the dispersion-corrected PM6 method using two different approximations: the two Pt(II) units are either placed adjacent or separately in the stack (Figures S11 and S12, Supporting Information). According to the calculations, the presence of two adjacent Pt(II) units imposes a more restricted conformation of the Pd(II) units, which agrees well with the formation of stiffer fibers for the mixture. On the other hand, the intercalation of isolated Pt(II) units in the stacks of **1** appears to induce a more disorganized molecular arrangement, thus suggesting a less favorable elongation process.

To gain deeper insights into this intriguing supramolecular co-assembly process, several mixing ratios **1/2** were further investigated. An overview of all the examined cooling curves reveal that an increment of the molar fraction of **1** shifts the T_e towards higher values (Figures 3a and b). The plot of T_e versus the molar fraction of **1** yields a linear progression, which is indicative of an efficient co-nucleation process at any ratio. Closer scrutiny of all these mixtures using AFM and DLS discloses the formation of only one type of supramolecular structure

(either nanodisks or fibers) or a mixture of the two depending on the ratio. For example, mixtures with a large excess of Pt(II) (80%–90% of **2**) lead to the exclusive formation of nanodisks, whereas solely nanofibers are formed at higher contents of Pd(II) (80–90% of **1**) (Figure S14, Supporting Information). These results can be explained by the presence of a single transition in the corresponding cooling curves. This is most pronounced for the 1:9 and 9:1 mixtures (Figure 3a), the curve shapes of which are almost identical to those of the complexes in isolation. In sharp contrast, the behavior of the mixtures with no significant excess of either component (3:7, 4:6, 6:4, and 7:3) bears close resemblance to the equimolar mixture, showing two-step cooling curves (Figure 3a) and consequently the coexistence of both aggregates (Figures 3c and d and Figure S15 in the Supporting Information).[17] Thus, careful selection of the temperature and mixing ratio allowed us to control the outcome of the supramolecular co-assembly. Our findings are in perfect agreement with the early prediction made by Isaacs and co-workers and the subsequent work in the field of self-sorting:[18] "*self-sorting is most efficient when the mixed components are present at the same concentration*".[18a]

In summary, we have elucidated the statistical supramolecular co-assembly of two structurally related π-conjugated Pd(II) and Pt(II) complexes in decane. Distinct nanostructures with a comparable pseudo-parallel molecular arrangement were observed for the systems in isolation (fibers for Pd(II) and nanodisks for Pt(II)). Self-sorting studies show a molar ratio-dependent degree of co-assembly that proceeds for all mixtures by a statistical co-nucleation event. While an excess of any of the complexes yields only one type of nanostructure (only fibers ([Pd(II)] ≫ [Pt(II)]) or nanodisks ([Pt(II)] ≫ [Pd(II)]) by a single-step co-assembly process, mixtures with similar ratios form Pd(II)-rich co-assembled fibers as well as residual self-sorted nanodisks in a stepwise manner. Although this self-sorting behavior may be characteristic of this particular type of metal-based π-systems, our results represent an efficient method to control the outcome of supramolecular copolymers by a statistical co-nucleation approach.
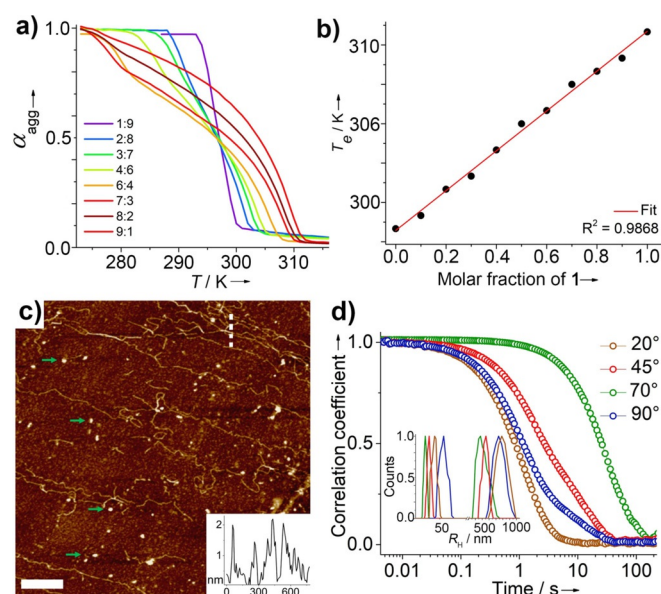
Figure 3. a) Plots of α_{agg} versus T at several mixing ratios at 52 μm in decane from 363 to 273 K (1 K min⁻¹). b) Plot of T_e versus molar fraction of **1** extracted from the spectra shown in (a). c) AFM image of the 4:6 mixture of **1**+**2** showing the coexistence of fibers and nanodisks (selected nanodisks are marked with green arrows). This sample was prepared by spin-coating at 273 K onto silicon wafer (scale bar = 500 nm). Inset: cross-section analysis corresponding to the white-dashed line shown in (c). d) Normalized size distribution obtained from the autocorrelation functions of the 4:6 mixture of **1**+**2** at different angles.

Acknowledgements

Conflict of interest

The authors declare no conflict of interest.

[1] T. D. Nguyen, B. Qiao, M. O. de la Cruz, *Proc. Natl. Acad. Sci. USA* **2018**, *115*, 6578–6583.
[2] L. Ii, K. Raghupathi, C. Song, P. Prassad, S. Thayumanavan, *Chem. Commun.* **2014**, *50*, 13417–13432.

[3] K. A. Davis, K. Matyjaszewski, *Adv. Polym. Sci.* **2002**, *159*, 1–157.

[4] a) B. Adelizzi, A. Aloi, A. J. Markvoort, H. M. M. ten Eikelder, I. K. Voets, A. R. A. Palmans, E. W. Meijer, *J. Am. Chem. Soc.* **2018**, *140*, 7168–7175; b) B. N. S. Thota, X. Lou, D. Bochicchio, T. F. E. Paffen, R. P. M. Lafleur, J. L. J. van Dongen, S. Ehrmann, R. Haag, G. M. Pavan, A. R. A. Palmans, E. W. Meijer, *Angew. Chem. Int. Ed.* **2018**, *57*, 15592–15596; *Angew. Chem.* **2018**, *130*, 15818–15822; c) A. Das, K. Petkau-Milroy, G. Klerks, B. van Genabeek, R. P. M. Lafleur, A. R. A. Palmans, E. W. Meijer, *ACS Macro Lett.* **2018**, *7*, 546–550; d) K. K. Zhang, M. C.-L. Yeung, S. Y.-L. Leung, V. W.-W. Yam, *Proc. Natl. Acad. Sci. USA* **2017**, *114*, 11844–11849; e) S. H. Jung, D. Bochicchio, G. M. Pavan, M. Takeuchi, K. Sugiyasu, *J. Am. Chem. Soc.* **2018**, *140*, 10570–10577.

[5] a) M. E. Robinson, D. J. Lunn, A. Nazemi, G. R. Whittell, L. De Cola, I. Manners, *Chem. Commun.* **2015**, *51*, 15921–15924; b) M. E. Robinson, A. Nazemi, D. J. Lunn, D. W. Hayward, C. E. Boott, M.-S. Hsiao, R. L. Harniman, S. A. Davis, G. R. Whittell, R. M. Richardson, L. De Cola, I. Manners, *ACS Nano* **2017**, *11*, 9162–9175.

[6] A. Das, G. Vantomme, A. J. Markvoort, H. M. M. ten Eikelder, M. Garcia-Iglesias, A. R. A. Palmans, E. W. Meijer, *J. Am. Chem. Soc.* **2017**, *139*, 7036–7044.

[7] For recent reports on (metallo)supramolecular OPE-based systems, see: a) M. Hifsudheen, R. K. Mishra, B. Vedhanarayanan, V. K. Praveen, A. Ajayaghosh, *Angew. Chem. Int. Ed.* **2017**, *56*, 12634–12638; *Angew. Chem.* **2017**, *129*, 12808–12812; b) E. Borré, J. F. Stumbé, S. B. Laponnaz, M. Mauro, *Angew. Chem. Int. Ed.* **2016**, *55*, 1313–1317; *Angew. Chem.* **2016**, *128*, 1335–1339; c) S. K. Albert, H. V. P. Thelu, M. Golla, N. Krishnan, R. Varghese, *Chem. Eur. J.* **2017**, *23*, 8348–8352; d) H. V. P. Thelu, S. K. Albert, M. Golla, N. Krishnan, S. B. Yamijala, S. V. Nair, S. M. Srinivasula, R. Varghese, *ChemistrySelect* **2016**, *1*, 5389–5396; e) J. P. Coelho, M. J. Mayoral, L. Camacho, M. T. Martín-Romero, G. Tardajos, I. López-Montero, E. Sanz, D. Ávila-Brande, J. J. Giner-Casares, G. Fernández, A. Guerrero-Martínez, *J. Am. Chem. Soc.* **2017**, *139*, 1120–1128.

[8] a) M. J. Mayoral, C. Rest, V. Stepanenko, J. Schellheimer, R. Q. Albuquerque, G. Fernández, *J. Am. Chem. Soc.* **2013**, *135*, 2148–2151; b) N. K. Allampally, M. J. Mayoral, S. Chansai, M. C. Lagunas, C. Hardacre, V. Stepa-

nenko, R. Q. Albuquerque, G. Fernández, *Chem. Eur. J.* **2016**, *22*, 7810–7816.

[9] a) H. Kar, G. Ghosh, S. Ghosh, *Chem. Eur. J.* **2017**, *23*, 10536–10542; b) Z. Gao, P. A. Korevaar, R. Zhong, Z. Wu, F. Wang, *Chem. Commun.* **2018**, *54*, 9857–9860.

[10] a) C. Rest, R. Kandanelli, G. Fernández, *Chem. Soc. Rev.* **2015**, *44*, 2543–2572; b) L. Tebben, C. Mück-Lichtenfeld, G. Fernández, S. Grimme, A. Studer, *Chem. Eur. J.* **2017**, *23*, 5864–5873.

[11] H. M. M. ten Eikelder, A. J. Markvoort, T. F. A. de Greef, P. A. J. Hilbers, *J. Phys. Chem. B* **2012**, *116*, 5291–5301.

[12] F. García, G. Fernández, L. Sánchez, *Chem. Eur. J.* **2009**, *15*, 6740–6747.

[13] A. Sakaguchi, K. Higashiguchi, K. Matsuda, *Chem. Commun.* **2018**, *54*, 4298–4301.

[14] D. S. Philips, A. T. Politi, K. K. Kartha, T. Krüger, R. Q. Albuquerque, G. Fernández, *Angew. Chem. Int. Ed.* **2019**, *58*, 4732–4736; *Angew. Chem.* **2019**, *131*, 4782–4787.

[15] a) J. Rezác, P. Hobza, *J. Chem. Theory Comput.* **2012**, *8*, 141–151; b) M. Lübtow, I. Helmers, V. Stepanenko, R. Q. Albuquerque, T. B. Marder, G. Fernández, *Chem. Eur. J.* **2017**, *23*, 6198–6205.

[16] M. I. Sluch, A. Godt, U. H. F. Bunz, M. A. Berg, *J. Am. Chem. Soc.* **2001**, *123*, 6447–6448.

[17] S. Whitelam, R. L. Jack, *Annu. Rev. Phys. Chem.* **2015**, *66*, 143–163.

[18] a) A. Wu, L. Isaacs, *J. Am. Chem. Soc.* **2003**, *125*, 4831–4835; b) M. M. S. Sempere, G. Fernández, F. Würthner, *Chem. Rev.* **2011**, *111*, 5784–5814; c) K. Aratsu, D. D. Prabhu, H. Iwawaki, X. Lin, M. Yamauchi, T. Karatsu, S. Yagai, *Chem. Commun.* **2016**, *52*, 8211–8214; d) H. Keisar, G. de Ruiter, A. H. Velders, P. Milko, A. Gulino, G. Evmenenko, L. J. W. Shimon, Y. Diskin-Posner, M. Lahav, M. E. van der Boom, *J. Am. Chem. Soc.* **2018**, *140*, 8162–8171.